



**HAL**  
open science

## Estimation of 3D geometrical properties of spheroid-like particle systems using projection images

Mathieu de Langlard, Fabrice Lamadie, Sophie Charton, Johan Debayle

### ► To cite this version:

Mathieu de Langlard, Fabrice Lamadie, Sophie Charton, Johan Debayle. Estimation of 3D geometrical properties of spheroid-like particle systems using projection images. ISIVC INTERNATIONAL SYMPOSIUM ON SIGNAL, IMAGE, VIDEO AND COMMUNICATIONS, Mines Saint-Etienne, Apr 2021, Saint-Etienne, France. pp.1-6, 10.1109/ISIVC49222.2021.9487552 . cea-03516334

**HAL Id: cea-03516334**

**<https://cea.hal.science/cea-03516334>**

Submitted on 7 Jan 2022

**HAL** is a multi-disciplinary open access archive for the deposit and dissemination of scientific research documents, whether they are published or not. The documents may come from teaching and research institutions in France or abroad, or from public or private research centers.

L'archive ouverte pluridisciplinaire **HAL**, est destinée au dépôt et à la diffusion de documents scientifiques de niveau recherche, publiés ou non, émanant des établissements d'enseignement et de recherche français ou étrangers, des laboratoires publics ou privés.

# Estimation of 3D geometrical properties of spheroid-like particle systems using projection images

Mathieu de Langlard

*Inria*

75012 Paris, France

mathieu.de-langlard@inria.fr

Fabrice Lamadie

*CEA, DES, ISEC, DMRC, Univ Montpellier*

Marcoule, France

fabrice.lamadie@cea.fr

Sophie Charton

*CEA, DES, ISEC, DMRC, Univ Montpellier*

Marcoule, France

sophie.charton@cea.fr

Johan Debayle

*CNRS, UMR 5307 LGF, Centre SPIN*

*Mines Saint-Etienne,*

42023 Saint-Étienne, France

debayle@emse.fr

**Abstract**—We propose a parametric method to estimate geometrical properties of a population of spheroid-like particles from 2D projection images. The method consists in, first, detecting the projection of the particles in the images, and then estimating the parameters of the supposed probability laws of the spheroids semi-axes using a Bayesian framework. Moreover, a new estimator of the Sauter mean diameter to assess the efficiency of two-phase flow processes, in the case of spheroid-like particle system, is proposed. Still in view to its practical use for the characterization of two-phase flows, the whole methodology is applied to a typical bubbly flow.

**Index Terms**—stereology, ellipsoids, Sauter mean diameter, projection, ellipse detection, approximate Bayesian computation

## I. INTRODUCTION

The characterization of particle systems encountered in multiphase flows is a fundamental step for the design and control of chemical processes. The experimental determination of the flow properties - such as the velocity fields, the size and shape distribution or the Sauter mean diameter (SMD) of the population of particles - requires rather sophisticated apparatus and techniques from the field of optics [1]. Typical signals acquired are 2D projection images, which then require proper processing to extract the information of interest.

Image analysis has become a powerful tool for monitoring particle systems as it enables to segment the particles projections on 2D experimental images and statistical analysis can be applied to retrieve information on the dispersed phase. Many segmentation algorithms [2]–[4] and modeling methods [5], [6] are reported to geometrically characterize particle systems in the case of sphere-like particles. However, for non-spherical ones, additional problems arise due to the projection mapping which results in a loss of information [7], [8]. Therefore, some assumptions have to be made regarding the particle system to compensate for this lack of information.

In many situations, ellipsoids arise as a simple, but realistic, model for given particles. They are frequently used as generalized model for droplets and/or bubbles, as this shape assumption covers a wide range of two-phase flow regimes [9]. Consequently, the observed 2D particle projections correspond to individual ellipses, or overlapping ellipses as the observation volume is generally large. Several segmentation algorithms have been proposed in the literature for overlapping ellipses in 2D images, see for example [8], [10]–[13]. However, very few stereological methods exist to infer the geometrical properties of the system from the projected ellipses [16].

In this paper, we propose a complete methodology to retrieve geometrical properties of a population of ellipsoids-like particles from its 2D projection images. More importantly, the proposed approach is able to fill the gap between the 2D set of projected ellipses and the corresponding 3D particle system of ellipsoids, providing assumptions are made on the shape and geometrical features of the particles - here we consider prolate ellipsoids, called *spheroids*.

The paper is organized as follows. In Section II, we recall briefly the detection algorithm for overlapping ellipses we detailed in [8]. In Section III, a Bayesian inference method is introduced to recover some 3D geometrical information on the spheroid-like particle system from the 2D detected ellipses. Then, a statistical method is described in Section IV to estimate the SMD. The method is applied to a bubbly flow in Section V.

## II. DETECTION OF THE PROJECTED ELLIPSES

The first step for the characterization of spheroid-like particle system is the segmentation of the projected ellipses. Previously we proposed an ellipse detection algorithm which has proved to be efficient to individualize ellipses from aggregates [8]. The algorithm consists in 1) detecting the *feature points* for each connected component of the binary

image. A feature point is a pixel of the boundary where the curvature function admits a local minimum ; 2) combining the *segments* of the boundary for each connected component. A segment is a part of the boundary between two successive feature points ; and 3) for each set of combinations, fitting ellipses on each group of segments and evaluate the overall fits using the goodness-of-fit criterion called *total average distance deviation*, denoted  $ADD_{\text{tot}}$  (see [8] for a precise definition of  $ADD_{\text{tot}}$ ). Consequently, for each connected component, the set of detected ellipses is the group of fitted ellipses which achieves the lowest  $ADD_{\text{tot}}$ .

A detection result is provided in Fig. 4 for a synthetic image of overlapping ellipses. The ellipses are uniformly oriented and located in the image, and are not allowed to intersect the border of the image. No constraint has been imposed on the overlapping ratio: ellipses can completely cover each other. The semi-axes are random variables whose distributions are uniform on the intervals  $[10, 20]$  and  $[15, 40]$  (unit is pixels). The ellipses cover approximately 22% of the total image surface, which is a typical value encountered in bubbles or droplets flows.

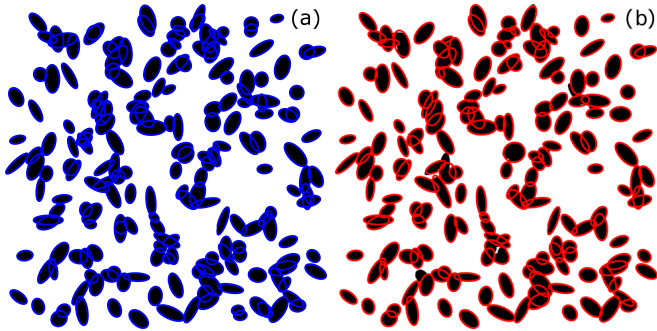


Fig. 1: Detection result on a simulated image of overlapping ellipses. In (a), the ground-truth population of ellipses. In (b), the detected ellipses with algorithm in [8].

The performances of our algorithm has been compared with two methods from the literature: the method proposed in [11] based on a classification, and the one proposed in [12] based on ellipse fitting. The three algorithms were applied on a set of 50 synthetic images similar to the one in Fig. 4. In total, approximately 9,000 ellipses were generated. Three usual quantitative metrics were used for comparison: the *true positive rate* (TPR), the *positive predictive value* (PPV), and the *Jaccard similarity coefficient* (JSC). The TPR and PPV are defined as followed:

$$TPR = \frac{TP}{TP + FN} \text{ and } PPV = \frac{TP}{TP + FP}, \quad (1)$$

where TP (True Positive) is the number of correctly segmented ellipses, FN (False Negative) is the number of missed ellipses, and FP (False Positive) is the number of incorrectly segmented ellipses. Starting from a binary image of the segmented ellipse  $E_s$ , the JSC is computed as

$$JSC = \frac{E_s \cap E_t}{E_s \cup E_t}, \quad (2)$$

where  $E_t$  is the binary map of the corresponding true ellipse. A segmented ellipse is considered correctly detected if there exists at least one true ellipse achieving  $JSC > 0.5$ . Among the true ellipses satisfying this constraint, the segmented ellipse is associated to the one achieving the highest JSC. The whole JSCs are generally averaged in a image in order to form a new metric, the AJSC (average JSC) which measures the mean segmentation performance in this image. The statistics obtained with the three methods are summarized in Table I, highlighting the efficiency of the method proposed in [8].

TABLE I: Performances of the proposed detection algorithm compared to two methods from the literature on a set of 50 simulated images of overlapping ellipses.

Algorithm	TPR	PPV	AJSC
Zafari, <i>et al.</i> [12]	0.84	0.85	0.79
Park, <i>et al.</i> [11]	0.67	0.87	0.71
de Langlard, <i>et al.</i> [8]	0.87	0.95	0.91

### III. 3D GEOMETRICAL CHARACTERIZATION

#### A. Modeling approach

Let  $\mathbf{y} = (\mathbf{y}_1, \mathbf{y}_2, \dots, \mathbf{y}_k)$  be the set of  $k \in \mathbb{N}^*$  detected ellipses where  $\mathbf{y}_i = (a'_i, b'_i)$  is the pair of semi-major and semi-minor axes of ellipse  $i \in \{1, \dots, k\}$ ,  $a'_i$  and  $b'_i$ , respectively. Note that there is only one orthogonal projection for each particle, and no information is given on the orientation of each ellipsoid. Therefore, reconstruction methods such as in [14], [15] are not applicable. However, some 3D geometrical properties can be estimated using a probabilistic setting.

We assume that the 3D particles are independent and identically distributed (i.i.d) realizations of a random ellipsoid of revolution about its semi-major axis  $a$  located at the origin, called *random spheroid*. The semi-minor axis  $b$  is defined by  $b = \epsilon a$ , where  $\epsilon$  is a random variable, called *flattening coefficient*, taking values in the unit interval  $[0, 1]$ . The observations  $\mathbf{y}_i = (a'_i, b'_i)$  are i.i.d realizations of the corresponding random projected ellipse with semi-major and semi-minor axes  $a'$  and  $b'$ , respectively. Two main assumptions follow:

- (A1) the particles are *isotropic*, i.e., there is no privileged orientation ;
- (A2) the semi-major axis  $a$  and flattening coefficient  $\epsilon$  follow the parametric probability laws  $\mathcal{F}_1$  and  $\mathcal{F}_2$ , respectively.

We denote  $\boldsymbol{\theta}_1 \in \mathbb{R}^{p_1}$  and  $\boldsymbol{\theta}_2 \in \mathbb{R}^{p_2}$  the respective parameter vectors of  $\mathcal{F}_1$  and  $\mathcal{F}_2$ , with  $p_1$  and  $p_2$  the number of parameters.

The aim of the method is to estimate the parameter vector  $\boldsymbol{\theta}_{\text{real}} = (\boldsymbol{\theta}_1, \boldsymbol{\theta}_2) \in \mathbb{R}^d$ , with  $d = p_1 + p_2$ , from the detected ellipses  $\mathbf{y}$ . A Bayesian framework is adopted, where the vector of parameter  $\boldsymbol{\theta}_{\text{real}}$  is considered as a realization of a random variable  $\Theta$ . The proposed method consists in finding the maximum *a posteriori* (MAP), i.e. the point value  $\boldsymbol{\theta}_{\text{MAP}}$  at which the posterior density function  $f(\cdot|\mathbf{y})$  is maximal. The

value  $\theta_{\text{MAP}}$  is then used as an estimator of  $\theta_{\text{real}}$ . From the Bayes formula, we have

$$f(\theta|\mathbf{y}) \propto l(\mathbf{y}|\theta)f(\theta), \quad (3)$$

where  $l(\cdot|\theta)$  is the probability density function of the projected ellipse semi-axes given a realization  $\theta$  of the random parameter vector  $\Theta$ , and  $f(\cdot)$  the *a priori* marginal probability density function of  $\Theta$ . We denote  $\mathcal{L}(\theta; \mathbf{y})$  the corresponding likelihood function.

Note that the joint distribution of the projected semi-axes of the particles is equal to the joint distribution of the projected semi-axes of the random spheroid with its axes used as the coordinate system and the projection direction being uniformly distributed on the unit sphere of  $\mathbb{R}^3$ . This equivalence is due to (A1) and to the i.i.d hypothesis for the particles. In [16], we proved that the likelihood function  $\mathcal{L}(\cdot; \mathbf{y})$  is not analytically tractable, hence, the posterior density cannot be easily maximized. Therefore, a numerical approach is required to first approximate the posterior density, and to compute an approximation of the MAP.

### B. Algorithm

A class of methods, called *approximate Bayesian computation* (ABC) methods, were introduced when the likelihood is not available in analytical form, see [18]. The simplest approach of ABC is based on a rejection technique by bypassing the calculation of the likelihood function. Only samples according to the conditional distribution of the observations given the set of parameters are required. If  $\mathbf{y} \sim l(\cdot|\theta)$ , then the proposed rejection method follows the three steps below:

- 1) sample  $\theta' \sim f(\cdot)$  ;
- 2) sample  $\mathbf{y}' \sim l(\cdot|\theta')$  ;
- 3) accept  $\theta'$  if  $\rho(S(\mathbf{y}'), S(\mathbf{y})) \leq \delta$ .

In the third step,  $S : \mathbb{R}^{2 \times k} \rightarrow \mathbb{R}_+^s$  is a function which calculates a set of  $s$  statistics on the  $\mathbf{y}$  data (*e.g.* mean, standard deviation, etc.) and the function  $\rho : \mathbb{R}^s \times \mathbb{R}^s \rightarrow \mathbb{R}^+$  measures the difference between the statistics of the simulated data  $\mathbf{y}'$  and those observed  $\mathbf{y}$ . If  $\theta'$  is accepted, it is a sample from the posterior distribution conditionally to  $\rho(S(\mathbf{y}'), S(\mathbf{y})) \leq \delta$ , *i.e.* from  $f(\cdot|\rho(S(\mathbf{y}'), S(\mathbf{y})) \leq \delta)$ . When  $\delta \rightarrow 0$ , we sample conditionally to the summary statistics of the observed data, *i.e.* from  $f(\cdot|S(\mathbf{y}))$ . Moreover, when the set of summary statistics  $S$  is *Bayes sufficient* (see [18], page 128), the approximate posterior density  $f(\cdot|\rho(S(\mathbf{y}'), S(\mathbf{y})) \leq \delta)$  converges to the true posterior  $f(\cdot|\mathbf{y})$  when  $\delta \rightarrow 0$ . However, the algorithm becomes ineffective in practice if  $\delta$  is too small as it results to a systematic rejection of all the  $\theta'$  proposals.

Given the set of  $n$  samples  $\theta_{1:n} = (\theta_1, \dots, \theta_n)$  from  $f(\cdot|\rho(S(\mathbf{y}'), S(\mathbf{y})) \leq \delta)$  (see [16] for practical consideration of the sampling algorithm), a kernel density estimator of  $f(\cdot|\rho(S(\mathbf{y}'), S(\mathbf{y})) \leq \delta)$  is obtained with

$$\hat{f}_n(\theta|\rho(S(\mathbf{y}'), S(\mathbf{y})) \leq \delta) = \frac{|H|^{-1/2}}{n} \sum_{i=1}^n K\left(H^{-1/2}(\theta - \theta_i)\right), \quad \forall \theta \in D, \quad (4)$$

where  $K$  is a kernel (a symmetric non-negative real-value integrable function whose integral equals 1 on  $\mathbb{R}^d$ ) and  $H$  is the so-called  $4 \times 4$  *bandwidth matrix* of the kernel density estimator with determinant  $|H|$ .

The non-parametric estimator in (4) can be maximized. Its maximum  $\theta_{\text{AMAP}}$ , called the *approximate maximum a posteriori* (AMAP), can serve as an approximation of  $\theta_{\text{MAP}}$ . Asymptotic properties of the *approximate maximum a posteriori* estimator can be found in [19]. Finally, the main steps of the algorithm is summarized in Algorithm 1. For the computation of the bandwidth matrix  $H$ , see [16].

---

### Algorithm 1 Estimation of the AMAP

---

- 1) Obtain  $n$  samples  $\theta_{1:n}$  from  $f(\cdot|\rho(S(\mathbf{y}'), S(\mathbf{y})) \leq \delta)$ .
  - 2) Construct the kernel density estimator  $\hat{f}_n(\cdot|\rho(S(\mathbf{y}'), S(\mathbf{y})) \leq \delta)$  using (4).
  - 3) Compute the maximum  $\hat{\theta}_{\text{AMAP}}$  of  $\hat{f}_n(\cdot|\rho(S(\mathbf{y}'), S(\mathbf{y})) \leq \delta)$  using an optimization algorithm.
- 

### C. Numerical tests

Several parameters may influence the quality of the AMAP estimator: the tolerance parameter  $\delta$ , the choice of summary statistics  $S$  and the number of samples  $n$ . Some numerical tests have been undertaken to quantify the impact of these parameters for a specific scenario.

We consider a random spheroid with a semi-major axis  $a$  following a Gamma law  $\Gamma(\tau, \nu)$  with shape and scale parameters  $\tau = 4$  and  $\nu = 0.05$ , and a flattening coefficient  $\epsilon$  following a truncated Gaussian law  $\text{tr}\mathcal{N}(0.85, 0.1; 1/2, 1)$  restricted to the interval  $[1/2, 1]$ , of mean 0.85 and standard deviation 0.1. The true set of parameters is  $\theta_{\text{real}} = (\mu_1, \sigma_1, \mu_2, \sigma_2)$ , where  $\mu_1 = \tau \times \nu = 0.2$ ,  $\sigma_1 = \sqrt{\tau \times \nu^2} = 0.1$ ,  $\mu_2 = 0.85$  and  $\sigma_2 = 0.1$ . A number of  $k$  realizations of the oriented random spheroid are sampled. Each realization  $i \in \{1, \dots, k\}$  is projected to obtain the set of  $k$  projected semi-axes,  $\mathbf{a}' = (a'_1, \dots, a'_k)$  and  $\mathbf{b}' = (b'_1, \dots, b'_k)$ . The AMAP estimator is computed from  $\mathbf{a}'$  and  $\mathbf{b}'$ .

The  $\rho$  function which measures the deviation between the statistics of the sampled semi-axes and the observations is defined by

$$\rho : \mathbb{R}^s \times \mathbb{R}^s \rightarrow \mathbb{R}_+ \\ (x, y) \mapsto \max_{1 \leq i \leq s} \left( \left| \frac{x_i}{y_i} - 1 \right| \right).$$

This function was initially proposed in [17]. A natural choice of statistics  $s$  is the mean and standard deviation of the semi-major axis and those of the flattening coefficient of the projected ellipses, hence, four statistics are considered.

First, the effect of decreasing values of  $\delta$  have been tested: 0.8, 0.6, 0.4 and 0.2. In each case, we sampled 20 times from the approximate posterior distribution  $\hat{f}_n(\cdot|\rho(S(\mathbf{y}'), S(\mathbf{y})) \leq \delta)$ , and computed the AMAP estimator for each sample. The sample size is  $n = 50,000$  and the number of observed ellipses is  $k = 4,000$ . Fig. 2 gives the violin plots of the AMAP estimator for the four parameters. In each graph, the horizontal

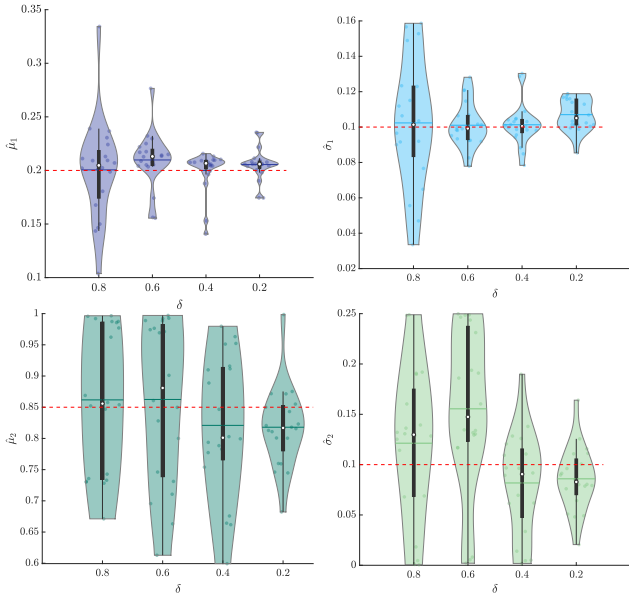


Fig. 2: Performances of the AMAP estimator with respect to the tolerance  $\delta$  for  $n = 50,000$  and  $k = 4,000$ . The mean and the median of the estimations are plotted within the violin plots in horizontal lines and white circles respectively. The target values are represented in red dashed lines.

line within the violin plots corresponds to the mean of the 20 estimations, while the median is highlighted with white circle, and the actual values of the target parameter are represented by the red dashed lines. A decrease of the dispersion of the distribution is evidenced as  $\delta$  decreases. The distribution tends to be more concentrated around the corresponding theoretical values. This is expected as  $\hat{f}_n(\cdot | \rho(S(\mathbf{y}'), S(\mathbf{y})) \leq \delta)$  is a better approximation of  $f(\cdot | \mathbf{y})$  when  $\delta$  decreases. Besides, the mean absolute percentage error (mape) for  $\delta = 0.2$  is less than 10% for  $\mu_1$ ,  $\sigma_1$  and  $\mu_2$ .

The corresponding error is however higher when considering the standard deviation of the flattening coefficient  $\sigma_2$ . One possible explanation is that the chosen summary statistics are not fully informative for the posterior distribution. This is confirmed with the result of the second numerical test when adding one more statistics: a fifth statistic, defined as the average area of the projected ellipses, is added to the four initial ones. We then observed a decrease of the mape for all four parameters with also a decrease of the statistical dispersion. On the contrary, if we removed the statistic on the standard deviation of the flattening coefficient of the projected ellipses - then only three statistics remain - we observed a significant deviation on the estimated parameters, especially for  $\mu_2$ . For more details on the numerical tests, see [16].

#### IV. ESTIMATION OF THE SAUTER MEAN DIAMETER

##### A. Definition

The SMD,  $d_{32}$ , is generally used to characterize two-phase flows composed of polydisperse populations of spherical particles, i.e., population of particles with different radii. The

SMD represents the radius of the particles of a monodisperse system which has the same total volume  $V_{\text{tot}}$  and total surface  $S_{\text{tot}}$  of the polydisperse one.

In the discrete and finite case, the polydisperse system is composed of particles with  $N$  different diameters  $d_j$ , where  $j \in \{1, \dots, N\}$ . The SMD is given by (see [20])

$$d_{32} = \frac{\sum_{j=1}^N n_j d_j^3}{\sum_{j=1}^N n_j d_j^2}, \quad (5)$$

where  $n_j$  is the number of particles of diameter  $d_j$ , which is equivalent to

$$d_{32} = 6 \frac{V_{\text{tot}}}{S_{\text{tot}}}. \quad (6)$$

##### B. Estimator for spheroids

Equation (6) can be used to get an estimator of the SMD, denoted  $\hat{d}_{32}$ , in the case of random spheroid-like particle systems such as the one in Section III. For random particle systems,  $V_{\text{tot}}$  and  $S_{\text{tot}}$  should naturally be replaced in (6) by  $\bar{V}_{\text{tot}}$  and  $\bar{S}_{\text{tot}}$ , i.e., the mean total volume and mean total surface of the particle system within the sampling window  $W$ .

It is assumed that the semi-major axis  $a$  and the flattening coefficient  $\epsilon$  have both continuous probability distributions with third order moment. Moreover, the mean number of particles per unit volume,  $\lambda$ , is independent on the space coordinates (we neglect edge effects due to the tank wall). Then, we have

$$\bar{V}_{\text{tot}} = V_{\text{obs}} \times \bar{V} \quad \text{and} \quad \bar{S}_{\text{tot}} = V_{\text{obs}} \times \bar{S}, \quad (7)$$

where  $V_{\text{obs}}$  is the volume of  $W$ ,  $\bar{V}$  and  $\bar{S}$  are the mean volume and mean surface area, respectively, of the particle system per unit volume. Moreover, by definition we have

$$\bar{V} = \lambda \mathbb{E}[V_p] \quad \text{and} \quad \bar{S} = \lambda \mathbb{E}[S_p], \quad (8)$$

where  $\mathbb{E}[V_p]$  and  $\mathbb{E}[S_p]$  are the mean volume and mean surface area of a particle, respectively. After replacing in (6), the constants cancel out and it comes

$$d_{32} = 6 \frac{\mathbb{E}[V_p]}{\mathbb{E}[S_p]}. \quad (9)$$

Replacing  $V_p$  and  $S_p$  by the expression of the volume and surface area of a prolate ellipsoid, and after some simplifications, the SMD is rewritten as

$$d_{32} = \frac{4(\mu_2^2 + \sigma_2^2) \mathbb{E}[a^3]}{(\mu_1^2 + \sigma_1^2)(\mu_2^2 + \sigma_2^2 + \mathbb{E}[\epsilon \arcsin(e)/e])}. \quad (10)$$

Consequently, the following estimator,  $\hat{d}_{32}$ , is proposed for the SMD in the case of prolate spheroid-like particle systems:

$$\hat{d}_{32} = \frac{4(\hat{\mu}_2^2 + \hat{\sigma}_2^2) \left. \frac{d^3 \widehat{M}_a(t)}{dt^3} \right|_{t=0}}{(\hat{\mu}_1^2 + \hat{\sigma}_1^2) \left( \hat{\mu}_2^2 + \hat{\sigma}_2^2 + 1/N_s \sum_{i=1}^{N_s} [\epsilon_i \arcsin(e_i)/e_i] \right)}, \quad (11)$$

where:

- $(\hat{\mu}_1, \hat{\sigma}_1, \hat{\mu}_2, \hat{\sigma}_2)$  are the estimators of the means and standard deviations of  $a$  and  $\epsilon$ ;

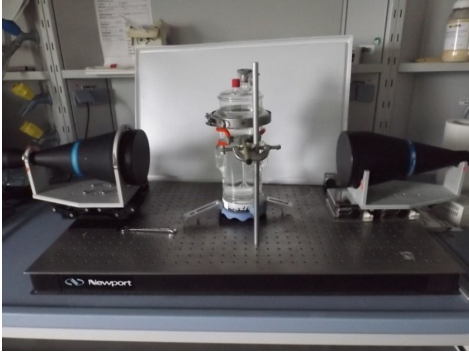


Fig. 3: Experimental setup of the bubbly flow.

- $\widehat{M}_\alpha$  is the moment generating function under the probability law of the semi-major axis ;
- $e_i = \sqrt{1 - \epsilon_i^2}$ , where  $\epsilon_i$  is a sample of the flattening coefficient. Then,  $1/N_s \sum_{i=1}^{N_s} [\epsilon_i \arcsin(e_i)/e_i]$  is the Monte-Carlo estimator of  $\mathbb{E}[\epsilon \arcsin(e)/e]$ , where  $N_s$  is the number of samples.

## V. APPLICATION

The flow takes place in a vertical glass cylinder of height 250 mm and diameter 100 mm, with two opposite planar optical windows in order to minimize light distortions. The tank is filled with deionized water with a volume of about 1L, and air is injected at the bottom through a sintered glass disk (with pore size in the range 4090 nm). Due to buoyancy, bubbles are rising in the liquids, pass in front of the windows and freely escape the cylinder at the top. The gas flow-rate is  $Q = 10\text{L/h}$ . The optical setup consists in a green collimated light-source, a bi-telecentric lens (from Optoengineering<sup>TM</sup>) and a high resolution and high dynamic CMOS camera (1.1 MPixel, 12 bits). Acquisitions are conducted at 50 fps, with an exposure time of  $1/60,000\text{s}$  in order to “freeze” the bubbles motion. The spatial resolution is  $1024 \times 1024$  pixels where 100 pixels corresponds to 1.72mm. Such a configuration, associating bi-telecentric lens and collimated light, is particularly suitable for two-phase flow observation as it provides high contrast images. A photograph of the experimental set-up is provided in Fig. 3.

The preprocessing and binarization procedure is standard and consists of the following steps: 1) a crop to remove the vignetting effect on the image edges, 2) a binarization using the Otsu’s method, and 3) a morphological area opening to remove very small objects ( $\leq 100$  pixels) considered as noise and measurement artifacts. The ellipse detection algorithm of Section II was applied to a set of 100 preprocessed experimental images. A typical experimental image and the corresponding detected ellipses are provided in Fig. 4. Note that the minus-sampling method is used to remove edge-effects, see [21].

More than 1000 ellipses have been detected from the measured images. The Bayesian inference method of Section III was applied using these detected ellipses. We assume

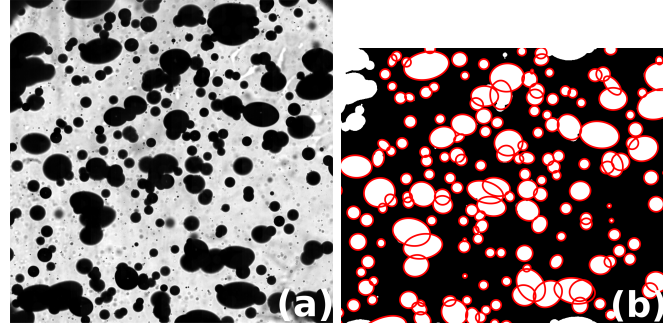


Fig. 4: Result of the detection algorithm on a typical projection image of the bubbly flow. (a) Typical image of the bubbly flow. (b) The detected ellipses in red with algorithm in [8].

TABLE II: Estimations of some 3D geometrical properties of the population of bubbles.

3D properties	Estimations
$\widehat{\lambda}$ ( $\text{mm}^{-3}$ )	0.00733
$\widehat{\mu}_1$ (mm)	0.43
$\widehat{\sigma}_1$ (mm)	0.26
$\widehat{\mu}_2$ (mm)	0.73
$\widehat{\sigma}_2$ (mm)	0.34
$\widehat{d}_{32}$ (mm)	1.16

that the semi-major axis follow a Gamma law with mean  $\mu_1$  and standard deviation  $\sigma_1$  and the flattening coefficient a truncated Gaussian law on the interval  $[0, 1]$  with mean  $\mu_2$  and standard deviation  $\sigma_2$ . From a statistical analysis of the detected ellipses, we remark that approx. 22% of the ellipses can be considered as perfect disk ( $\epsilon \geq 0.98$ ) and approx. 65% exhibit flattening coefficient higher than 0.9. This results highlights that, on average, the shape of the bubbles tends to be close to that of a sphere. Therefore, we assume for the Bayesian inference in Section III that the parameter  $\mu_2$  is Beta distributed with parameter  $\alpha = 5$  and  $\beta = 2$ . Thus, the prior density function  $f(\theta)$  is designed as

$$f(\theta) = f(\mu_2) = \frac{\Gamma(\alpha + \beta)}{\Gamma(\alpha)\Gamma(\beta)} \mu_2^{\alpha-1} (1 - \mu_2)^{\beta-1}, \quad (12)$$

where  $\Gamma$  is the Gamma function. Moreover, the numerical experiments undertaken in Section III suggest to choose the tolerance parameter  $\delta = 0.2$ , the number of samples  $n = 10000$  and the set of five statistics.

As the volume of observation is known, the estimator  $\widehat{\lambda}$  of the particle density can be easily computed. Moreover, using the Bayesian inference procedure of Section III, we estimate the mean and the standard deviation of the semi-major axis ( $\widehat{\mu}_1$  and  $\widehat{\sigma}_1$ ) and the ones of the flattening coefficient ( $\widehat{\mu}_2$  and  $\widehat{\sigma}_2$ ). The estimators  $\widehat{\mu}_1$ ,  $\widehat{\sigma}_1$ ,  $\widehat{\mu}_2$  and  $\widehat{\sigma}_2$  are the means of the AMAP estimator over 20 runs. Furthermore, the SMD of the population of bubbles can be estimated by  $\widehat{d}_{32}$  using (11). These values are presented in Tab. II.

Although the exact properties of the bubbly flow are not known in this case, we can compare the  $\widehat{d}_{32}$  in Tab. II

with another estimator of the SMD, denoted  $\widehat{d}_{32}^{\text{lit}}$ , which is sometimes used in the literature [10]. It is computed from the area-equivalent diameter, i.e.,

$$\widehat{d}_{32}^{\text{lit}} = \frac{\sum_j n_j d_{j,eq}^3}{\sum_j n_j d_{j,eq}^2}, \quad (13)$$

where  $n_j$  is the number of detected ellipses in the class  $j$  with area-equivalent diameter equal to  $d_{j,eq}$ . The area-equivalent diameter of a detected ellipse is the diameter of the disk having the same area of the detected ellipse. For the considered population of bubbles, we obtained  $d_{32}^{\text{lit}} = 1.32$  mm, hence a relative difference of 14% with  $\widehat{d}_{32}$ . Unlike  $\widehat{d}_{32}$ , a major drawback of  $d_{32}^{\text{lit}}$  is that it does not hold any relevant 3D geometrical information on the population of bubbles. Indeed, there is no straightforward relationship between the area-equivalent diameter of the ellipses and the total volume or total surface of the population of bubbles. This lack of geometrical consistency for the SMD when using  $d_{32}^{\text{lit}}$  may explain the difference obtained when estimating it with  $\widehat{d}_{32}$ .

## VI. CONCLUSION

We proposed a complete methodology to estimate important 3D geometrical properties of spheroid-like particle systems encountered in two-phase flows, using 2D projection images. It consists in detecting the 2D projections of the particles in the images, and estimating the parameters of the semi-axes probability laws from these detections using a Bayesian framework. The main drawback of the Bayesian inference method is the assumption made on the probability laws of the semi-major axis and flattening coefficient of the particles. These probability laws are not known in practice. Therefore, we can only expect to estimate accurately the first order moments of the distributions. Some numerical tests have been undertaken in previous papers for validating the detection algorithm and the Bayesian inference method. However, it is very difficult to test and validate the full methodology on typical two-phase flows as the exact 3D properties of the particle system are not known.

Besides, we proposed a new estimator of the SMD which is an important characteristic for most particulate flow applications. For the considered bubbly flow, the comparison between the proposed estimator of the SMD and the one generally used in the literature suggests that some cares have to be taken. Unlike  $\widehat{d}_{32}$ , the SMD estimator  $\widehat{d}_{32}^{\text{lit}}$  cannot be used to characterize the efficiency of the flow as there is no straightforward geometrical relationship between the area-equivalent diameter of a projected ellipse and the volume or the surface area of the corresponding spheroid. This why for very elongated particles, i.e. whose shape deviates strongly from that of a sphere, the proposed SMD estimator  $\widehat{d}_{32}$  in (11) should be preferred.

## REFERENCES

[1] F. Lamadie, S. Charton, M. de Langlard, M. Ouattara, M. P. Sentis, J. Debayle, and F. Onofri, "Development of Optical Techniques for Multiphase Flows Characterization," ASME 2017 Fluids Engineering Division Summer Meeting, Hawaii, August 2017.

[2] L. Shen, X. Song, M. Iguchi, and F. Yamamoto, "A method for recognizing particles in overlapped particle images," *Pattern Recognition Letters*, vol. 21, pp. 21-30, January 2000.

[3] A. Khalil, F. Puel, Y. Chevalier, J.M. Galvan, A. Rivoire, A., and J. P. Klein, "Study of droplet size distribution during an emulsification process using in situ video probe coupled with an automatic image analysis," *Chemical Engineering Journal*, vol. 165, pp. 946-957, Decembre 2010.

[4] Y. Lau, N. Deen, and J. Kuipers, "Development of an image measurement technique for size distribution in dense bubbly flows," *Chemical Engineering Science*, vol. 94, pp. 20-29, May 2013.

[5] W. Kracht, X. Emery, and C. Paredes, "A stochastic approach for measuring bubble size distribution via image analysis," *International Journal of Mineral Processing*, vol. 121, pp. 6-11, March 2013.

[6] M. de Langlard, F. Lamadie, S. Charton, and J. Debayle, "A 3D stochastic model for geometrical characterization of particles in two-phase flow applications," *Pattern Recognition Letters*, vol. 37, pp. 233-247, September 2018.

[7] O. S. Ahmad, J. Debayle, and J-C. Pinoli, "A geometric-based method for recognizing overlapping polygonal-shaped and semi-transparent particles in gray tone images," *Pattern Recognition Letters*, vol. 32, pp. 2068-2079, September 2011.

[8] M. de Langlard, H. Al-Saddik, S. Charton, J. Debayle, and F. Lamadie, "An efficiency improved recognition algorithm for highly overlapping ellipses: Application to dense bubbly flows," *Pattern Recognition Letters*, vol. 101, pp. 88-95, January 2018.

[9] R. Clift, J. R. Grace, and M. E. Weber, *Bubbles, Drops, and Particles*. Dover Publications, 2005.

[10] W. H. Zhang, X. Jiang, and Y. M. Liu, "A method for recognizing overlapping elliptical bubbles in bubble image," *Pattern Recognition Letters*, vol. 33, pp. 1543-1548, September 2012.

[11] C. Park, J. Z. Huang, J. Y. Ji, and Y. Ding, "Segmentation, inference, and classification of partially overlapping nanoparticles," *IEEE Transactions on Pattern Analysis and Machine Intelligence*, vol. 35, pp. 669-681, Mars 2013.

[12] S. Zafari, T. Eerola, J. Sampo, H. Klviinen, and H. Haario, "Segmentation of overlapping elliptical objects in silhouette images," *IEEE Transactions on Image Processing*, vol. 24, pp. 5942-5952, December 2015.

[13] Y. Fu, and Y. Liu, "Development of a robust image processing technique for bubbly flow measurement in a narrow rectangular channel," *International Journal of Multiphase Flow*, vol. 84, pp. 21-228, September 2016.

[14] R. Noumeir, "Detecting three-dimensional rotation of an ellipsoid from its orthographic projections," *Pattern Recognition Letters*, vol. 20, pp. 585-590, June 1999.

[15] W. C. Karl, G. C. Verghese, and A. S. Willsky, "Reconstructing ellipsoids from projections," *CVGIP: Graphical Models and Image Processing*, vol. 56, pp. 124-139, March 1994.

[16] M. de Langlard, F. Lamadie, S. Charton, and J. Debayle, "Bayesian inference of a parametric random spheroid from its orthogonal projections," *Methodology and Computing in Applied Probability*, July 2020.

[17] J. K. Pritchard, M. T. Seielstad, A. Perez-Lezaun, and M. W. Feldman, "Population growth of human Y chromosomes: a study of Y chromosome microsatellites," *Molecular Biology and Evolution*, vol. 16, pp. 1791-1798, December 1999.

[18] S. A. Sisson, Y. Fan, and M. Beaumont, *Handbook of Approximate Bayesian Computation*. Chapman and Hall/CRC, 2018.

[19] F. J. Rubio, and A. M. Johansen, "A simple approach to maximum intractable likelihood estimation," *Electronic Journal of Statistics*, vol. 7, pp. 1632-1654, 2013.

[20] P. B. Kowalczyk, and J. Drzymala, "Physical meaning of the Sauter mean diameter of spherical particulate matter," *Particulate Science and Technology*, vol. 34, pp. 645-647, January 2016.

[21] J. Ohser, and K. Schloditz, *3D Images of Materials Structures: Processing and Analysis*. John Wiley & Sons, 2009.